Modulation of Microtubule Interprotofilament Interactions by Modified Taxanes

Ruth Matesanz,[†] Javier Rodríguez-Salarichs,[†‡] Benet Pera,[†] Ángeles Canales,[†§] José Manuel Andreu,[†] Jesús Jiménez-Barbero,[†] Wim Bras,[¶] Aurora Nogales,[‖] Wei-Shuo Fang,[**] and José Fernando Díaz[†*]

[†]Chemical and Physical Biology, Centro de Investigaciones Biológicas, Consejo Superior de Investigaciones Científicas CIB-CSIC, Madrid, Spain; [‡]Centro de Estudios Avanzados de Cuba, Carretera San Antonio, Valle Grande, La Lisa, Ciudad Habana, Cuba; [§]Departamento de Química Orgánica I, Facultad Ciencias Químicas, Universidad Complutense de Madrid, Madrid, Spain; [¶]Nederlandse Organisatie voor Wetenschappelijk Onderzoek (NWO), DUBBLE CRG/ESRF, Grenoble, France; [‖]Instituto de Estructura de la Materia, Consejo Superior de Investigaciones Científicas IEM-CSIC, Madrid, Spain; and [**]State Key Laboratory of Bioactive Substances and Functions of Natural Medicines, Institute of Materia Medica, Chinese Academy of Medical Sciences & Peking Union Medical College, Beijing, China

ABSTRACT Microtubules assembled with paclitaxel and docetaxel differ in their numbers of protofilaments, reflecting modification of the lateral association between $\alpha\beta$-tubulin molecules in the microtubule wall. These modifications of microtubule structure, through a not-yet-characterized mechanism, are most likely related to the changes in tubulin-tubulin interactions responsible for microtubule stabilization by these antitumor compounds. We have used a set of modified taxanes to study the structural mechanism of microtubule stabilization by these ligands. Using small-angle x-ray scattering, we have determined how modifications in the shape and size of the taxane substituents result in changes in the interprotofilament angles and in their number. The observed effects have been explained using NMR-aided docking and molecular dynamic simulations of taxane binding at the microtubule pore and luminal sites. Modeling results indicate that modification of the size of substituents at positions C7 and C10 of the taxane core influence the conformation of three key elements in microtubule lateral interactions (the M-loop, the S3 β-strand, and the H3 helix) that modulate the contacts between adjacent protofilaments. In addition, modifications of the substituents at position C2 slightly rearrange the ligand in the binding site, modifying the interaction of the C7 substituent with the M-loop.

INTRODUCTION

Fully assembled microtubules are long hollow cylinders ~25 nm in diameter composed of laterally associated tubulin protofilaments. The number of protofilaments per microtubule can range from 10 to 18, although the number is usually 13 in vivo (1). In contrast, this number is variable in vitro and depends on the experimental conditions. It should be stressed that the actual protofilament number is heterogeneous and follows a distribution. In fact, the number of protofilaments is given as an average figure (1).

Taxanes are a class of antitumor drugs in clinical use (2) that exert their cytotoxic action through the microtubule cytoskeleton. Paclitaxel (Fig. 1) and its chemical relatives, such as docetaxel, belong to this group of drugs (3). Taxanes prevent microtubule disassembly by activation of GDP-bound tubulin (4,5). They were the first available class of compounds with microtubule-stabilizing-agent (MSA) activity.

Several models have been proposed (see Wu et al. (6) for a review) to explain the structural mechanisms of microtubule assembly. The most simplistic of these proposes one-by-one addition of tubulin dimers to the growing end of a nucleus (7). In our case, the structural pathway of MSA-induced microtubule assembly has been studied using small-angle x-ray scattering (SAXS) (8). Under the biochemical conditions of this study, and in the presence of MSA, the first structural step of the assembly involves head-to-tail oligomerization of tubulin dimers in the presence of Mg^{+2} ions to form linear oligomers, called protofilaments. These linear oligomers laterally associate to form the nucleus (a process mediated by the MSA), which grows until the number of protofilaments is sufficient to display cylindrical morphology, with the correct interprotofilament angle (Fig. 1). This so-called interprotofilament angle is defined as the average angle between protofilaments in the cylindrical cross section (see Fig. 2 *A*, *inset*). The nucleus then elongates by incorporating new tubulin subunits to the growing end of the cylinder. This model is compatible with previous observations of intermediate sheet structures (9) and with the observed fast growth of existing microtubules from elongation of sheetlike structures at the growing ends (10). However, we should point out that although the MSA-induced microtubule assembly, employed in this study, can be considered as a model system of the physiological GTP-induced microtubule assembly, the exact mechanism of GTP-induced tubulin assembly both in vivo and in vitro is controversial (11,12), and microtubule formation may proceed through a different structural pathway.

In earlier studies on the interaction of taxanes with microtubules, we found that the structure of paclitaxel-induced microtubules is different from the structure of those assembled in the absence of this drug (13). In the presence of

Submitted June 27, 2011, and accepted for publication November 3, 2011.

This article is dedicated to the memory of our late colleague Prof. Francisco Amat-Guerrí, in whose laboratory Flutax-1, Flurax-2, and HexaFlutax were originally synthesized.

*Correspondence: fer@cib.csic.es

Editor: Kathleen B. Hall.

0006-3495/11/12/2970/11 $2.00

doi: 10.1016/j.bpj.2011.11.005

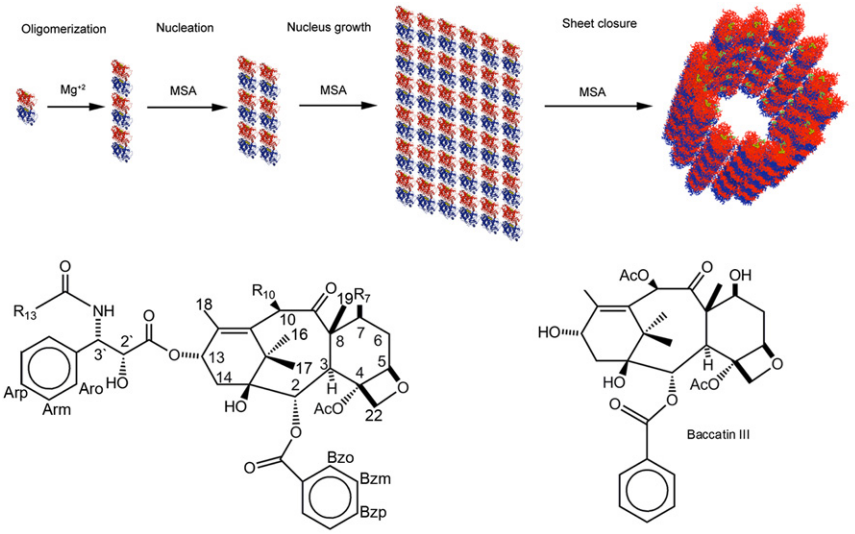

R13	R10	R7	m		R13	R10	m	
Aryl	Acetyl	Hydroxyl	-H	Paclitaxel	Aryl	Acetyl	-H	Flutax-1, Flutax-2 and Hexaflutax
Aryl	Acetyl	Hydroxyl	-OCH_3	Chitax-11				
Aryl	Acetyl	Hydroxyl	-N_3	Chitax-12				
Aryl	Hydroxyl	Hydroxyl	-H	Chitax-15				
tert-butyl	Hydroxyl	Hydroxyl	-H	Docetaxel				
tert-butyl	Acetyl	Hydroxyl	-H	Chitax-21				
tert-butyl	Propionyl	Hydroxyl	-N_3	Chitax-40				
2-butene	Acetyl	Hydroxyl	-H	Cephalomannine				
2-butene	Acetyl	Hydroxyl	-OCH_3	Chitax-13				
2-butene	Acetyl	Hydroxyl	-N_3	Chitax-14				
2-butene	Propionyl	Hydroxyl	-H	Chitax-18				
2-butene	Propionyl	Hydroxyl	-OCH_3	Chitax-19				
2-butene	Propionyl	Hydroxyl	-N_3	Chitax-20				
2-butene	Hydroxyl	Hydroxyl	-H	Chitax-17				
2-butene	Hydroxyl	Propionyl	-H	Chitax-1				
2-butene	Hydroxyl	Propionyl	-OCH_3	Chitax-5				
2-butene	Hydroxyl	Propionyl	-N_3	Chitax-4				
tert-butyl	Acetyl	Hydroxyl	-H*	Chitax-42				

* The benzoyl moiety at C2 has been replaced by benzamide

C7 side chain of Flutax-1, Flutax-2 and Hexaflutax

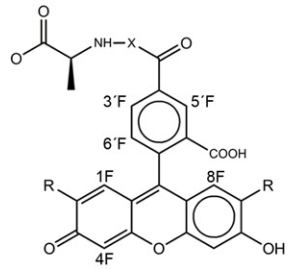

	R	X
Flutax-1	-H	-
Flutax-2	-F	-
Hexaflutax	-H	$CO(CH_2)_5NH$

FIGURE 1 (*Upper*) Structural pathway of MSA-induced microtubule assembly, adapted from Díaz et al. (8). (*Lower*) Chemical structures of the compounds employed in this study.

paclitaxel, microtubules assembled with an average of 12.1 protofilaments (13), which is rather different from the average number of protofilaments found in vitro (13.4). Strikingly, when assembled in the presence of docetaxel, the microtubules have an average protofilament number identical to that found in the absence of drugs (14). The most straightforward explanation for this observation would be that these compounds can alter the way in which protofilaments interact laterally. In addition, the exchange of paclitaxel for docetaxel, or the addition of Flutax-2 (a chemically modified fluorescent analog) to microtubules preassembled in the absence of drugs resulted in rapid changes (within a timescale of <1 min) in the number of protofilaments (8,15,16). Therefore, the mechanism of MSA-induced assembly should modify the interprotofilament angle and subsequently the average number of microtubule protofilaments.

Although high-resolution electron diffraction located the main paclitaxel binding site on the internal surface of microtubules (17), rather remote from the interprotofilament space, our studies (18–21) have provided evidence that another binding site exists for MSAs. This site is in the vicinity of residue T220 of β-tubulin (at the outer surface of the pore in the microtubule wall). On the other hand, it has been described that binding of paclitaxel to the luminal site of microtubules facilitates the interaction between the S7-H9 loop (M-loop) of β-tubulin and the H1-S2 loop of the adjacent subunit (17). This enhanced M-loop-H1-S2-loop interaction has been proposed as one of the key reasons for the microtubule-stabilizing activity of paclitaxel (22). In both cases (binding in the outer surface of the pore or binding at the luminal site), MSA-tubulin interactions take place close to the interprotofilament region, so it is not unreasonable to imagine that they should modify the corresponding angle and, thus, the microtubule structure.

Herein, we have employed SAXS to determine the average microtubule diameter and the number of

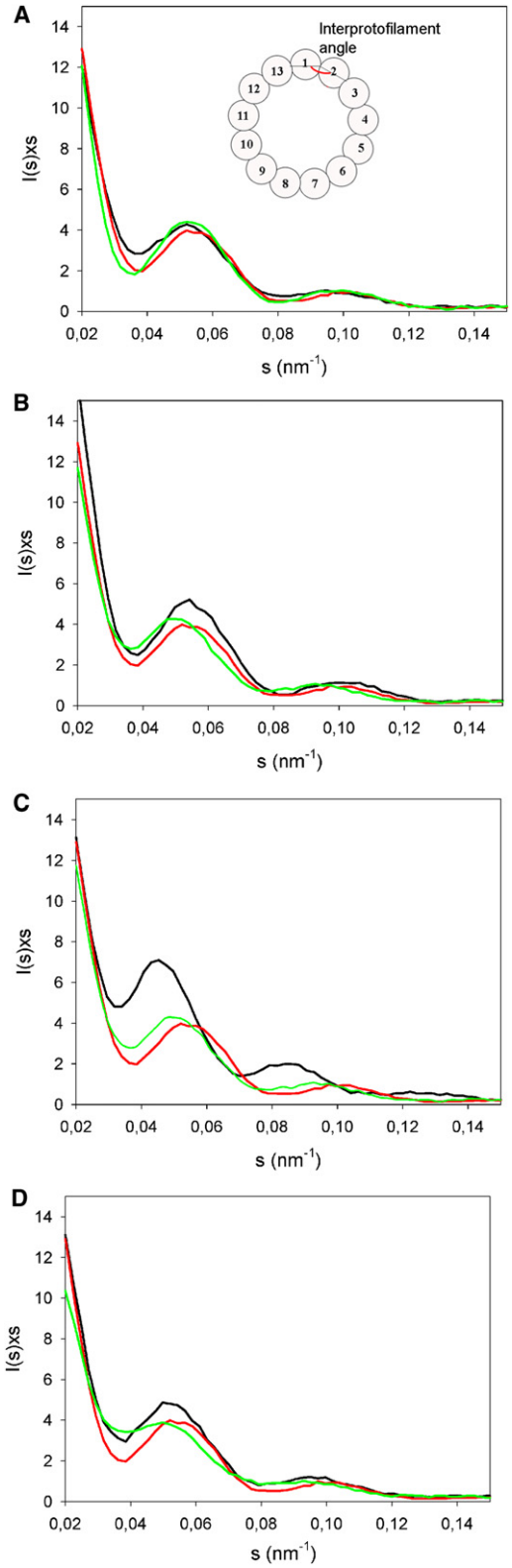

FIGURE 2 Effect of single modifications in the different side chains on the SAXS profiles of microtubules assembled in the presence of different taxanes. (*A*) Effect of changes in the C13 side chain. SAXS profiles of microtubules assembled in the presence of Chitax-21 (*black line*), cephalomannine (*red* or *dark gray line*), and paclitaxel (*green* or *light gray line*). (*Inset*) Schematic drawing of a microtubule indicating the interprotofilament angle. (*B*) Effect of changes in the C10 side chain. SAXS profiles of microtubules assembled in the presence of Chitax-18 (*black line*), cephalomannine (*red* or *dark gray line*), and Chitax-17 (*green* or *light gray line*). (*C*) Effect of changes in the C7 side chain. SAXS profiles of microtubules assembled in the presence of Chitax-1 (*black line*), cephalomannine (*red line*), and Chitax-17 (*green line*). (*D*) Effect of changes in the C2 side chain. SAXS profiles of microtubules assembled in the presence of Chitax-13 (*black line*), cephalomannine (*red* or *dark gray line*), and Chitax-14 (*green* or *light gray line*).

protofilaments. By comparing SAXS data of microtubules assembled in the presence of a series of different modified taxanes (Fig. 1), it has been possible to shed light on the mechanisms involved in the modification of the microtubule structure by these ligands. On this basis, the goal of this work has been to obtain insights, at molecular and atomic resolution, into the mechanisms of MSA-induced microtubule assembly by understanding how ligands with different chemical functional groups may modify the interactions between protofilaments. These events are probably related to those that modulate tubulin-tubulin interactions and induce microtubule assembly. Therefore, taxane derivatives with different sizes and shapes have been selected from a library of active compounds (23). In particular, a number of molecules were selected for our study based on different observations; since the first differences in the observed number of protofilaments involved paclitaxel and docetaxel, which mainly differ in the substitutions at the C13 lateral chain (in the eastern part of the molecule), these two molecules and related analogs were initially selected for our study. However, between these two key molecules there is also one smaller modification at position 10 (in the northern part of the taxane core), which was also chosen for further exploration. On the other hand, we also decided to explore the consequences of the chemical differences between paclitaxel, Flutax-1, and Flutax-2, which involve the C7 lateral chain (in the northeastern part of the taxane core). In addition, the effect of modifications at the C2 side chain (in the southern part) has also been evaluated, since these modifications have a significant influence on the binding of taxanes to microtubules (23).

MATERIALS AND METHODS

Ligands and protein

Purified calf brain tubulin and chemicals were synthesized and used as described (5,16,18,23,24). Baccatin III was from Sigma-Aldrich (St. Louis, MO). All compounds were dissolved at 50 mM concentration in D_6-DMSO.

X-ray scattering measurements

Tubulin was equilibrated in a buffer of 10 mM sodium phosphate, 1 mM EDTA, 0.1 mM GTP, pH 7.0, through a Sephadex G-25 medium column (25 × 9 mm), and the protein was centrifuged for 20 min at 90,000 × *g* in a TLA120.2 rotor in an Optima TLX centrifuge (Beckman, Palo Alto, CA) to remove aggregates. The tubulin concentration was then determined

spectrophotometrically as described previously (25). $MgCl_2$ (7 mM) and up to 1 mM GTP were added to the sample (final pH 6.7), the desired ligand or DMSO (vehicle) in a 10% stoichiometric excess over the protein concentration was added, and the samples were incubated for 20 min at 37°C and kept at 25°C before recording the scattering patterns.

SAXS data collection was performed either at BM26B station (DUBBLE) of the European Synchrotron Radiation Facility in Grenoble (France) or at a Bruker (Rheinstetten, Germany) NANOSTAR system (see Supporting Material for details).

The low-angle x-ray scattering pattern of microtubules in solution can be described as the Fourier transform of a hollow cylinder. To a first approximation, the intensity is given by the zeroth-order Bessel function, $|J_0(qR)|^2$, where q is the scattering angle and R the cylinder radius (26). The position of the first scattering maximum is therefore a sensitive measure for the radius of the microtubule, via the relation $J_{01} = (1.22/2R)$, since in a solution scattering pattern these are not distorted due to overlap between the higher-order diffraction maxima of the helical lattice (13,14).

The differences in diameter between microtubules assembled in the presence of different taxanes can be interpreted, to a good approximation, as changes in the average number of protofilaments making up the cylinder wall.

NMR sample preparation and experiments

The samples of the ligands bound to microtubules were prepared, measured at 310 K in D_2O on Bruker AVANCE 500 MHz or 700 MHz spectrometers and analyzed as described previously (21). Off-rate constants in the range 1–200,000 s^{-1} were tested to fit the experimental saturation transfer difference (STD) effects and transferred nuclear Overhauser enhancement (TR-NOE) intensities. Optimal agreement was achieved for $k_{off} = 90\ s^{-1}$ for cephalomannine, Chitax-1, Chitax-4, and Chitax-17, and $k_{off} = 110\ s^{-1}$ for Flutax-2.

Docking and molecular dynamics calculations

Docking of the ligands was performed as described (21) (see Supporting Material for details).

Autodock poses with the best fitting between experimental and calculated STD values were refined by using molecular dynamics (MD) simulations performed with AMBER 9 (27) (500-ps equilibration time, 2-ns acquisition time). For each compound, 100 structures were saved along the last nanosecond of the MD trajectory. The predicted STD values of each structure were obtained with CORCEMA-ST and the average STD values of these 100 structures were considered for comparison against the experimental data. Finally, the normalized root mean-square deviation (NRMSD) between these average STD values and the experimental STD were calculated for each proton of the ligand.

The volume of the solvent-excluded surface (V-SES) by the side chains of the taxanes was calculated using the MSMS program (28) to calculate the excluded surface and the Chimera program (29) to calculate the volume under the excluded surface.

RESULTS

SAXS determination of the sizes of the ligand-induced microtubules

Tubulin assembly was induced in the presence of the different ligands, and the corresponding SAXS profiles were recorded for each microtubule population. Fig. 2 shows a comparison of the profiles for selected molecules that differ in a single position of the taxane side chain. From these profiles, the positions of the first-order Bessel function maxima J_{01} were determined, and appropriate controls were performed to assure that the position of Jn peak (proportional to the distance between the center of the protofilaments) remained constant in all cases. From these data, the average microtubule diameters and average protofilament number were calculated (Table 1).

Except for the case of Chitax-14, in which the valleys are remarkably less pronounced, indicating a larger proportion of open microtubular sheets (8), the width of the peaks and the ratio between the maximum of the J_{01} peak and the minimum between J_{01} and J_{02} is very similar for all the compounds studied. This indicates that the distribution of protofilament numbers and the proportion of open microtubular sheets should be similar for all ligand-induced microtubules and also similar to those previously described by electron microscopy (1,8,13,14).

Effect of the modification of the ligand size, at selected positions, in the microtubule structure

The effects of single point changes of the taxane molecule on the interprotofilament contacts can be then calculated from the changes in the number of protofilaments (Table 2). When the SAXS patterns of paclitaxel-induced

TABLE 1 Structural data of the ligand-induced microtubules

Compound	J_{01} (nm^{-1})*	Mean helical radius (nm)†	Average protofilament number‡
Baccatin III	0.0595 ± 0.0006	10.3 ± 0.2	11.3 ± 0.3
Cephalomannine	0.0535 ± 0.0002	11.4 ± 0.1	12.6 ± 0.1
Paclitaxel	0.0518 ± 0.0004	11.8 ± 0.1	13.0 ± 0.1
Docetaxel	0.0480 ± 0.0005	12.7 ± 0.2	14.0 ± 0.2
Chitax-1	0.0455 ± 0.0002	13.4 ± 0.1	14.8 ± 0.1
Chitax-4	0.0443 ± 0.0008	13.8 ± 0.3	15.2 ± 0.3
Chitax-5	0.0435 ± 0.0005	14.0 ± 0.1	15.5 ± 0.1
Chitax-11	0.0498 ± 0.0003	12.2 ± 0.1	13.5 ± 0.1
Chitax-12	0.0501 ± 0.0003	12.2 ± 0.1	13.4 ± 0.1
Chitax-13	0.0518 ± 0.0004	11.8 ± 0.1	13.0 ± 0.1
Chitax-14	0.0493 ± 0.0002	12.4 ± 0.1	13.6 ± 0.1
Chitax-15	0.0504 ± 0.0003	12.1 ± 0.1	13.3 ± 0.1
Chitax-17	0.0501 ± 0.0003	12.2 ± 0.1	13.4 ± 0.1
Chitax-18	0.0543 ± 0.0004	11.2 ± 0.1	12.4 ± 0.1
Chitax-19	0.0476 ± 0.0003	12.8 ± 0.1	14.1 ± 0.1
Chitax-20	0.0503 ± 0.0004	12.1 ± 0.1	13.4 ± 0.1
Chitax-21	0.0513 ± 0.0006	11.9 ± 0.2	13.1 ± 0.3
Chitax-40	0.0521 ± 0.0005	11.7 ± 0.2	12.9 ± 0.2
Flutax-1	0.0460 ± 0.0002	13.3 ± 0.1	14.6 ± 0.1
Flutax-2	0.0460 ± 0.0002	13.3 ± 0.1	14.6 ± 0.1
Hexaflutax	0.0446 ± 0.0003	13.7 ± 0.1	15.1 ± 0.1

*Values indicate the position of the J_{01} maxima in the scattering profiles obtained from three independent measurements. Fitting of the peaks was done using the curve-fitting software tool TableCurve2D 5.01 (Systat Software, Richmond, CA). The error is the error of the best fit.

†Values are the helical radii estimated from the positions of the first subsidiary maxima of the J_0 Bessel function $J_{01} = 1.22/2R$ (26).

‡Calculated from the mean helical radius and the microtubule interprotofilament spacing (5.7 nm) (14).

TABLE 2 Changes in protofilament numbers due to single point modifications

Modification type	Modification	Compounds	Change in pf number	Average change*	ΔV-SES (Å^3)
C2	Benzoyl to 3-N_3 benzoyl	P→12	+0.4	+0.7 ± 0.2	+35
		C→14	+1.0		
		18→20	+1.0		
		1→4	+0.4		
	Benzoyl to 3-OCH_3 benzoyl	P→11	+0.5	+0.8 ± 0.3	+24
		C→13	+0.4		
		18→19	+1.7		
		1→5	+0.7		
C7	-OH to propionyl	17→1	+1.4	+1.4	+52
	-OH to Fluorescein	P→Flutax-1	+1.6	+1.6	+366
	-OH to diFluoro-Fluorescein	P→Flutax-2	+1.6	+1.6	+375
	-OH to $(CH_2)_6$-Fluorescein	P→Hexaflutax	+2.1	+2.1	+453
C10	-OH to Acetyl	17→C	−0.8	−0.7 ± 0.2	+48
		15→P	−0.3		
		D→21	−0.9		
	-OH to Propionyl	17→18	−1.0	−1.0	+53
C13	PTX→CPH	P→C	−0.4	−0.2 ± 0.2	−15
		11→13	−0.5		
		12→14	+0.2		
		15→17	+0.1		
	PTX→DXL	P→21	+0.1	+0.1	+11
	CPH→DXL	C→21	+0.5	+0.2 ± 0.3	+8
		17→D	+0.6		
		20→40	−0.5		
	PTX→None	P→BIII	−1.7	−1.7	−256

*Errors, where applicable, are the standard error.
pf, protofilament; V-SES, volume of solvent-excluded surface; PTX, paclitaxel side chain; DXL, Docetaxel side chain; CPH, Cephalomannine side chain; P, paclitaxel; D, Docetaxel; C, Cephalomannine; BIII, baccatin III.

microtubules (Fig. 2 *A*, *green line*) are compared with patterns of microtubules assembled in the presence of Chitax-21 and cephalomannine (paclitaxel equivalents with specific modifications only at the C13 side chain) (Fig. 2 *A*, *black* and *red lines*, respectively), the differences in the position of the J_{01} maxima fell within the experimental error (Table 2). The same result was obtained for the rest of the taxanes with single point modifications at the C13 side chain (Table 2). Only the removal of the C13 side chain (from paclitaxel to baccatin III) resulted in a large decrease of 1.7 units in the average number of protofilaments.

The result indicates that the change in microtubule structure observed between paclitaxel-induced and docetaxel-induced microtubules (13,14) was actually not due to the modification at the side chain. However, the results point toward a strong influence of the volume of the side chain in the interaction with the binding site. In fact, the size of the two side chains involved is nearly the same as shown by the calculation of the change in V-SES by the side chain (Table 2) (size change if phenyl is exchanged for tert-butyl +11 Å^3). Exchange of these two side chains for a different one with a similar size (butylen) (size change if phenyl is exchanged for butylen, −15 Å^3) does not result in an appreciable change in the protofilament number, whereas removing the side chain that results in a volume change of −256 Å^3 results in a large decrease of the average number of protofilaments.

It is therefore evident that the difference observed between the structure of the microtubules induced by paclitaxel and that of the microtubules induced by docetaxel should arise from the difference of the group at position 10 (acetyl group versus a free OH moiety, for paclitaxel and docetaxel, respectively), and corresponds to a volume decrease of 42 Å^3

An increase in volume at position 10 resulted in a small but consistent decrease in the number of protofilaments of the induced microtubules. The introduction of acetyl (cephalomannine; Fig. 2 *B*, *red line*) or propionyl (+53 Å^3) groups (Chitax-18; Fig. 2 *B*, *black line*) at position 10 resulted in a decrease of the microtubule diameter compared with Chitax-17 (Fig. 2 *B*, *green line*) (Table 2). When an acetyl group was introduced as a single point modification at position 10, the average decrease in the number of protofilaments was 0.7. When a propionyl group was introduced, the decrease corresponded to 1.0 protofilament.

An opposite effect is seen for the other group in the north face of the molecule, C7, which also points toward the inter-protofilament space in both binding sites. The introduction of bulky groups, such as fluorescein (+366 Å^3) and difluoro-fluorescein (+375 Å^3) (Flutax-1 and Flutax-2), at this position instead of the free hydroxyl resulted in a large increase in the microtubule diameter (16). However, the relatively large size of these groups may result in additional interactions. Therefore, a further comparison experiment was also

performed for analogs bearing a smaller propionyl side chain (+53 Å^3). Thus, the effect observed could be compared to that monitored for the equivalent change at position 10.

The introduction of a propionyl side chain at C7 (Chitax-17 → Chitax-1) resulted in an increase in the diameter of the microtubules (Fig. 2 *C*, *green* and *black lines*, respectively) equivalent to 1.4 extra protofilaments. Accordingly, this variation was similar to that observed for the introduction of the fluorescein moieties mentioned above, with 1.6 extra protofilaments (see Table 2). It is interesting that the introduction of a bulkier group such as 7-hexaflutax (+453 Å^3) resulted in the largest change in diameter observed, corresponding to 2.1 protofilaments, as also shown in Table 2.

Since the south face of the molecule and, more precisely, the benzyl moiety at the C2 position of the taxane ring strongly influences the interactions of these compounds with the luminal site (23) and, very probably, also with the pore site (20), we have studied the modifications at C2 that highly modulate the binding affinity. In both cases, the C2-modified molecules with groups at the meta position of the ring, which increase the binding affinity, amplified the microtubule diameter (Table 2). An average increase of 0.7 units was observed for compounds bearing an azide substituent, which added an extra 35 Å^3 (-N_3, Chitax-14; Fig. 2 *D*, *black line*) and an average increase of 0.8 units, for the methoxy-containing analogs, which added 24 Å^3 (-OCH_3, Chitax-13; Fig. 2 *D*, *green line*).

NMR and molecular modeling

Three-dimensional models of the ligands bound to the two alternative binding sites (the luminal and pore sites) were obtained to understand the effects, at the structural level, of ligand binding to microtubules. A combined NMR and modeling approach was employed when NMR experiments could be performed. Unfortunately, taxane solubility problems precluded general use of the combined procedure. However, in the case of docetaxel (21,23), paclitaxel, chitax-42, and flutax-2 (this work), it was possible to obtain NMR-based information regarding the bioactive conformations and the binding epitopes of the ligands, and this information was employed as a guide for the modeling procedures.

STD experiments detect magnetization transfer from the protein to a bound ligand. Only bound ligands show STD signals and, as in any NOE-type experiment, the STD effect observed depends on the distance between the protons of the protein and those of the ligand, thus providing a useful tool to detect the ligand epitope and to structurally probe the binding site. This information is of paramount importance to improve the docking models. However, there are kinetic requirements for these experiments to be successful. Indeed, STD and TR-NOESY experiments (which permit deduction of the bioactive conformation of the ligand) require a fast off-rate in the relaxation timescale. Therefore, as previously discussed, the characteristic slow dissociation of ligands from the luminal site in the microtubules precludes observation of the TR-NOESY and STD signals from the ligand when it is bound to this site (23). As a matter of fact, the calculated STD profiles of the taxanes bound to the luminal site cannot reproduce those experimentally determined (21). Thus, the NMR-based information for these systems can only be employed to model the pore-bound poses.

Three model compounds were selected for the construction of the model average STD profile of taxanes. Paclitaxel and docetaxel were selected as lead compounds in the series, whereas Chitax-42 (a low-affinity compound with a modified linker at C2) was chosen to determine whether all active taxanes bind to microtubules in the same way. Flutax-2 (16) was also measured as an example of those analogs bearing bulky probes at C7. STD and TR-NOESY data were acquired for paclitaxel, Chitax-42, and Flutax-2 (experimental data are shown in Fig. 3 A, and a higher-resolution version of the TR-NOESY spectra is available in Fig. S1 in the Supporting Material). Docetaxel data were taken from our previous studies (21,23). Regarding the taxane part of the molecules, the molecular conformation deduced from TR-NOESY spectra was found to be identical to that previously described for docetaxel (21,23).

Flutax-2 was modeled in the pore site (Fig. 3 *B*) using its experimentally measured STD profile (Fig. 3 *C*), as described in Materials and Methods. The NRMSD factor of the best model was 19.38%, in between those obtained for the previously published models of docetaxel (9.9%) and discodermolide (22.4%) bound to microtubules (21). Given the bulky group at C7, which may be involved in additional interactions with the binding site, STD effects of Flutax-2 protons were not employed to build the model average STD profile for the common protons of paclitaxel, which was later used to model the nonfluorescent ligands.

Four selected ligands (cephalomannine, Chitax-1, Chitax-4, and Chitax-17, which differ in single points at C7 (Chitax-17 and cephalomannine), C10 (Chitax-17 and Chitax-1), and C2 (Chitax-1 and Chitax-4)) were modeled in the pore site employing the model average STD profile of taxanes. These ligands were chosen because of their possible influence on the microtubule interprotofilament contacts described above. As in the case of Flutax-2, the compounds were first docked into the pore site, and they produced different poses. After this procedure, the geometries of the docking poses were employed to calculate the expected STD profiles (30). The poses were then classified by comparing their expected STD values to those of the model average taxane (Fig. 3 *D*), and their geometries were compared to those experimentally determined for docetaxel (23) and to those estimated for the T-Taxol conformation (31). Based on the conservation of the TR-NOESY profile, only those models in which the structure of the ligand was compatible with either of these geometries were further considered (Table S1). The NRMSD between the STD estimations was considered to quantify the similarities, as described in the Materials and Methods. The

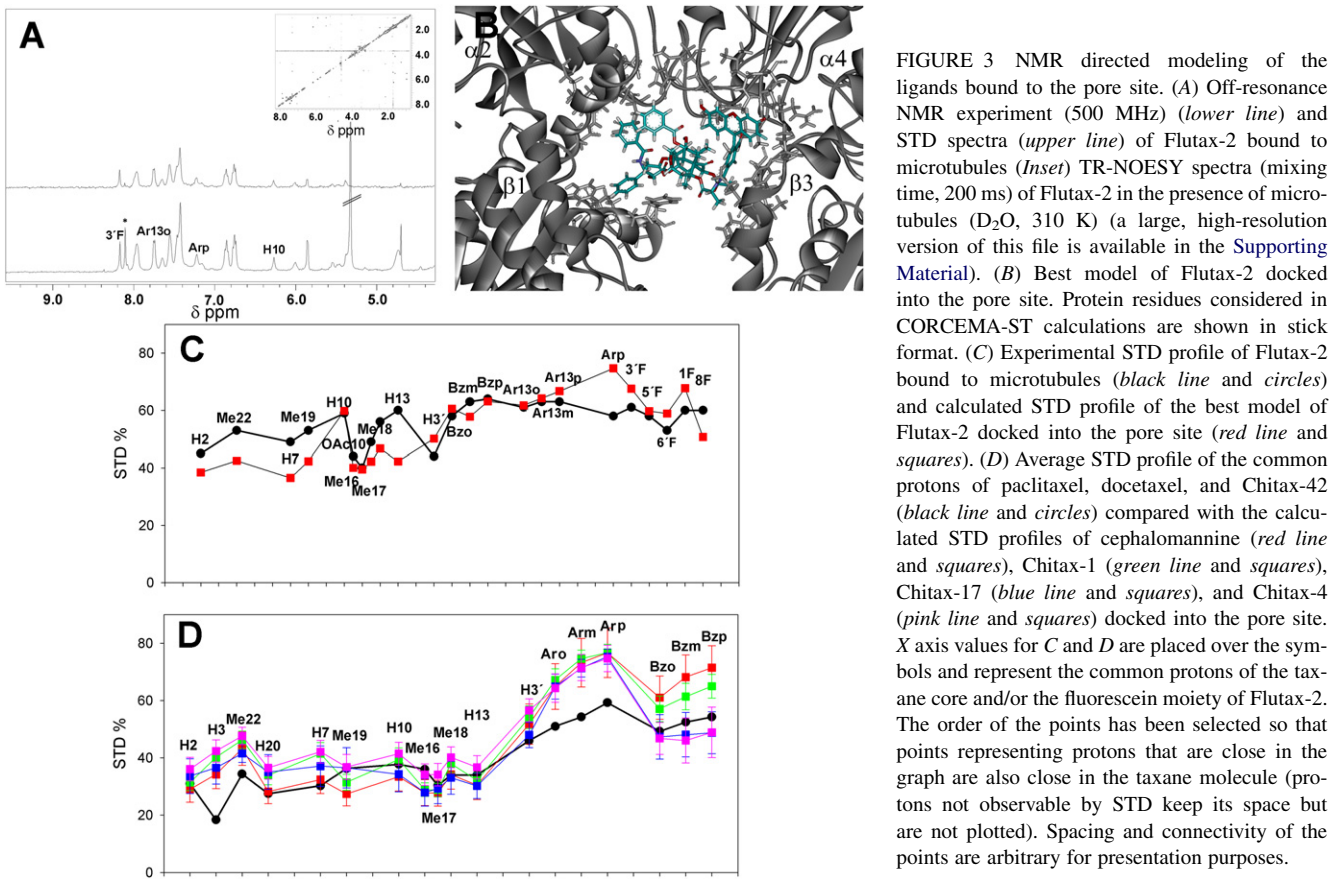

FIGURE 3 NMR directed modeling of the ligands bound to the pore site. (*A*) Off-resonance NMR experiment (500 MHz) (*lower line*) and STD spectra (*upper line*) of Flutax-2 bound to microtubules (*Inset*) TR-NOESY spectra (mixing time, 200 ms) of Flutax-2 in the presence of microtubules (D_2O, 310 K) (a large, high-resolution version of this file is available in the Supporting Material). (*B*) Best model of Flutax-2 docked into the pore site. Protein residues considered in CORCEMA-ST calculations are shown in stick format. (*C*) Experimental STD profile of Flutax-2 bound to microtubules (*black line* and *circles*) and calculated STD profile of the best model of Flutax-2 docked into the pore site (*red line* and *squares*). (*D*) Average STD profile of the common protons of paclitaxel, docetaxel, and Chitax-42 (*black line* and *circles*) compared with the calculated STD profiles of cephalomannine (*red line* and *squares*), Chitax-1 (*green line* and *squares*), Chitax-17 (*blue line* and *squares*), and Chitax-4 (*pink line* and *squares*) docked into the pore site. *X* axis values for *C* and *D* are placed over the symbols and represent the common protons of the taxane core and/or the fluorescein moiety of Flutax-2. The order of the points has been selected so that points representing protons that are close in the graph are also close in the taxane molecule (protons not observable by STD keep its space but are not plotted). Spacing and connectivity of the points are arbitrary for presentation purposes.

NRMSD values obtained (cephalomannine, 18.93%; Chitax-1, 18.26%; Chitax-17, 16.23%; and Chitax-4, 18.79%) and the models were between those determined for the best structures previously obtained for docetaxel and discodermolide (21) (Fig. 4, *A–C*). The ligands were found to bind between the tubulin β-subunit, close to the luminal site (β1, following the Magnani nomenclature (32)), and the α-subunit of the next dimer in the protofilament (α2; see the cyan structure in Fig. 5 *A* of Canales et al. (21)), as previously described for docetaxel (21). However, although the location of the binding site was similar to that described by Magnani (but rather different from that found by Freedman et al. (33), close to subunits β1 and β4), the binding pose of the ligands was rather different from that described by Magnani (32).

Alternatively, the four ligands were modeled in the luminal binding site (1JFF model) (17) by direct docking of the geometries constructed from the TR-NOESY-determined docetaxel conformation (23), as previously described (34) (Fig. 4, *E–H*).

The geometries of the best docking poses were considered as initial structures for MD simulations. In this way, the influence of the different ligands on the interprotofilament contacts was evaluated. As hypothesized, the different chemical moieties at the peripheral substitutions made distinct and specific contacts with determined protein regions. Local perturbation of the conformations of the H3 and S3 elements of the β-tubulin subunit at the right side of the pore (orange subunit) was observed when the ligand was bound to the pore site (Fig. 4, *A–C*). Alternatively, perturbations in the topology of the β-tubulin M-loop, which contains the luminal site, were detected when the ligand was bound to this site (Fig. 4, *E–H*). These changes in the protein conformation are likely to result in variations of the interprotofilament contacts.

Fig. S2 shows the effect of the cephalomannine, Chitax-17, Chitax-1, and Chitax-4 series in the M-loop. They induced 12.6, 13.4, 14.8, and 15.2 protofilament-containing microtubules, respectively. It could be deduced that these molecules, especially cephalomannine and Chitax-17, induced the closing of the M-loop toward the luminal site, thus giving rise to the formation of microtubules with a low number of protofilaments.

DISCUSSION

To better understand the mechanism of MSA-induced microtubule assembly and why interprotofilament contacts and subsequently the microtubule structure are altered compared with GTP-induced assembly, different taxanes with groups of different sizes at selected positions were employed. We then observed how modification in the taxane

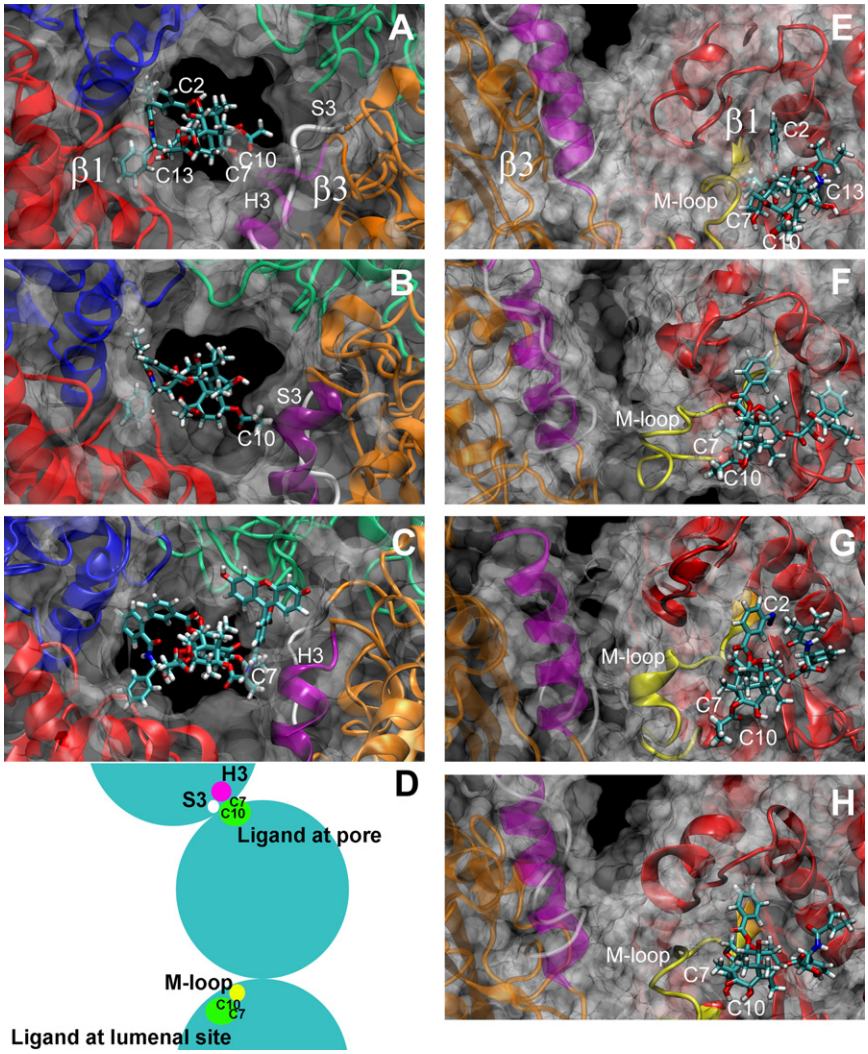

FIGURE 4 Models of ligands bound to microtubules. (*A–C*) Ligands bound to pore site: (*A*) cephalomannine; (*B*) Chitax-1; and (*C*) Flutax-2. Magenta, H3 helix of the β3-tubulin subunit; white, S3 of the β3-tubulin subunit. (*D*) Scheme of the interaction of the ligand at both binding sites with the structural elements responsible for the interprotofilament interaction. The scheme shows the positions of H3, S3, and the M-loop in the interprotofilament interface with respect to the two possible binding sites for the taxanes, as well as the substituents of the ligands that interact with them, altering the interprotofilament contacts. A ligand bound to the pore site will interact with H3 through the substituent at position C7, increasing the interprotofilament angle, and with S3 through the substituent at position C10, decreasing the angle. A ligand bound to the luminal site will interact with the M-loop through the substituent at position C10, producing the same effect as in the pore site. The microtubule is seen from the plus end. (*E–H*) Ligands bound to the luminal site: (*E*) cephalomannine; (*F*) Chitax-1; (*G*) Chitax-4; and (*H*) Chitax-17. Magenta, H3 helix of the β3-tubulin subunit; white, S3 of the β3-tubulin subunit; yellow, M-loop of the β1-tubulin subunit. Model structures are available in the Supporting Material.

shape is reflected in the microtubule structure, assuming it unlikely that the general features of the interaction of the ligand with the binding sites would be altered by these minor modifications. NMR-directed models of the formed complexes have been constructed to understand, at high resolution, how the different taxanes modify microtubule structure and cause stabilization. In this way, we have constructed a data-directed model of the interaction of taxanes with both the pore and luminal sites of microtubules, and of the conformational effects that binding to these sites produces in contacting tubulin subunits. Thus, the SAXS data, and the observed modifications in the number of protofilaments, can be discussed in terms of the NMR-directed docking models obtained.

How does ligand binding to the pore and luminal sites affect microtubule structure?

To properly understand the effects of changes in the ligand side chains on the interprotofilament structure, we carefully examined models of the complexes of the ligands with both binding sites. Our initial working hypothesis was that the interactions of the different taxane ligands with the pore binding site (19,35), located between the protofilaments, should be the one most likely involved in the modifications observed in the interprotofilament angle and thus in the average number of protofilaments of which the microtubule cylindrical structure is composed. In agreement with this hypothesis, the only compound known to bind exclusively to the microtubule pore, 7-hexaflutax (18,20), is the ligand that produces the largest effect on the microtubule structure.

Given the transient nature of the interaction of all taxanes except Hexaflutax with the pore site, it is only possible to determine the ratio of compound bound to each of the sites for the fluorescent compounds Flutax-1 (10% outer site) and Flutax-2 (1% outer site) (16). However, for docetaxel, STD and TR-NOESY NMR analysis of the ligand-receptor systems also indicates that a significant percentage of nonfluorescent taxanes would have to be bound to the pore site (23).

However, the strong difference between the ratios of binding of these three compounds—Flutax-1, Flutax-2,

and Hexaflutax—to both sites, as compared with the similarity of sizes of the groups (366, 375, and 453 $Å^3$, respectively) and the microtubules induced by these drugs (14.6, 14.6, and 15.1 protofilaments, respectively) suggests that either the effect exerted is through both luminal and pore sites or that only a small proportion of the ligand is enough to produce the effect on microtubule structure. Thus, to gain information about the specific effect, models of the interaction with both the pore and luminal sites have to be analyzed.

The results indicate that the main effect of ligands at both the pore site and the luminal site is due to modification of the size of groups at positions C7 and C10. The analysis of the 3D models of the ligands derived from NMR and docking simulations with O-substituents at the north face of the molecule (taxane positions C7 and C10) reveals a well-defined mode of interaction with the pore site. The groups at these positions strongly interact with the secondary H3 and S3 structure elements of the β-tubulin subunit at the adjacent protofilament, modifying their molecular conformations (Fig. 4 *D* and Fig. S2 *A*), whereas the positions that are relevant to the binding, C2 and C13, are oriented toward the center of the protofilament (Fig. 4). When no substituents are present at the hydroxyl groups at C7 and C10, the groups are exposed to the solvent, making favorable interactions with the water molecules, and in turn do not interact with the protein (accordingly, compounds with no substituents at the hydroxyl groups at C7 and C10, such as docetaxel, Chitax-15, and Chitax-17, have little influence on the microtubule diameter). It is fitting that when a hydrophobic group is present at this location, the protein rearranges its conformation to protect the nonpolar areas from the solvent. When the substitution takes place at C7, which is close to the surface of the pore, the H3 helix changes its topology, resulting in a conformation that is more compact the bigger the side chain is. This in turn results in protofilament-protofilament interactions with larger interprotofilament angles. Alternatively, for the C10-substituted analogs, the modified position is closer to the inner surface. In this case, the tubulin S3 strand rearranges to close the interprotofilament contacts in the inner part of the protein. This process involves a reduction in the interprotofilament angle, and thus, thinner microtubules, with fewer protofilaments, are formed. The effect on the pore structure can be clearly seen in Fig. 4. In the presence of cephalomannine (Fig. 4 *A*), which contains an acetyl group at position 10 and a hydroxyl at position 7, the H3 helix is not well structured (*magenta*) and is located far from the ligand. In contrast, when the C10 acetyl is removed and a propionyl group is introduced at C7 (Chitax-1 (Fig. 4 *B*)), the helix becomes stable and interacts with the ligand. A similar effect can be observed with Flutax-2 (Fig. 4 *C*).

The modeling indicates that when the ligands are bound to the luminal site, their influence is exerted through changes in the orientation of the tubulin M-loop (see Fig. 4, *D–G*, and Fig. S2 *B*). A similar effect was observed by Mitra and Sept (36) in a large-scale molecular simulation employing the T-taxol conformation (37). This indicates that, as previously proposed, the effect on this loop is one of the reasons for the microtubule stabilizing effect. Substitutions at taxane positions C7 and C10 produce different orientations of this secondary tubulin structure element. Different structures of the M-loop are observed when an acyl substituent is at position 10 (Fig. S2 *B*), as with cephalomannine (*yellow loop*), or when a large substituent is located at position 7, as with Chitax-1 (*green loop*). It is interesting that for nonsubstituted hydroxyl groups at C7 and C10 (as in Chitax-17), the M-loop adopts the intermediate orientation (Fig. S2 *B*, *white loop*) between those described above. Looking at the structural basis for the observed variations, the presence of the acyl substituent at position 10 induces changes in the orientation of the M-loop, which shifts inward due to contacts between the acyl moiety and Arg^{278} and Thr^{276}. These interactions result in the existence of closer contacts between protofilaments in the luminal part of the microtubule wall and therefore in smaller interprotofilament angles. Microtubules assembled in the presence of Chitax-17 resulted in a microtubule cylinder with an average of 13.4 protofilaments, whereas cephalomannine microtubules only contained 12.6 protofilaments. In contrast, the presence of substituents at taxane position 7 induced the outward shifting of the M-loop due to contacts between the acyl group and Gln^{282}. This alternative shift results in the assembly of microtubules with larger interprotofilament angles. In fact, Chitax-17 microtubules have 13.4 protofilaments, whereas Chitax-1 microtubules have 14.8.

The models of the ligands docked into both the pore and luminal binding sites (Fig. 4) indicate that the C13 side chain is not interacting with the loops responsible for the interprotofilament contacts. Thus, the large change observed in its absence should be the result of a different pose of baccatin III in the sites, farther away from the S3 and H3 loops in the pore site and from the M-loop in the luminal site.

The increase in volume of the meta group of the benzyl moiety at taxane position C2 produced alternative variations at other locations in the luminal binding pocket. As a key example, incorporation of an azide moiety at the C2 aromatic ring resulted in a closer interaction of the ligand with His^{229}, which has been proposed as the main reason for the observed increase in affinity (23). This intermolecular interaction slightly modified the presentation of the ligand and forced a large movement of the M-loop toward the interprotofilament space (Fig. S2 *B*, blue loop). This motion produced the concomitant change in the number of protofilaments, which increases from 14.8 for Chitax-1 to 15.2 for Chitax-4. This effect can also be easily observed by inspecting Fig. 4. In the presence of just a hydroxyl group (as for Chitax-17 (Fig. 4 *H*)), the M-loop packs closer to the ligand than it does in the presence of an acetyl group at position 7 (as for Chitax-1, Fig. 4 *F*). This effect is reinforced

with the addition of the N3 moiety to the aromatic ring at C2 (as for Chitax-4, fig. 4G).

CONCLUSIONS

The mechanisms of ligand-induced microtubule stabilization have been explored with a set of taxane analogs. These ligands modify the structure of these polymers by altering the interprotofilament contacts as detected by SAXS. Modeling protocols, assisted by NMR experiments, were used for different protein complexes containing ligands bound at the pore site or at the luminal site. The modeled 3D structures were employed to analyze the microtubule structural changes detected, providing plausible explanations for the structural influence of these compounds in modulating microtubule assembly.

Although it is not strictly possible to isolate the individual effects arising from ligand binding to the luminal or pore site, simulations indicate that the binding process strongly influences the interactions at three tubulin regions, with different well-defined secondary-structure elements. These regions, the S7-H9 loop (M-loop), helix H3, and the S3 strand (Fig. 4 *D*) have been described as key elements for interprotofilament interactions (17) and could be selectively targeted by employing the adequately designed analogs.

SUPPORTING MATERIAL

Methods, a table, references, two figures, and eight structures of the models presented are available at http://www.biophysj.org/biophysj/supplemental/S0006-3495(11)01317-8.

We thank Rhône Poulenc Rorer Aventis for supplying the docetaxel, Miss Jessica Field for editing and correcting the text, and Matadero Municipal Vicente de Lucas de Segovia for providing the calf brains for tubulin purification.

J.R.S. had a fellowship from Programa de Cooperación Científica entre el Ministerio de Ciencia, Tecnologías y Medio Ambiente de la República de Cuba (CITMA) y el Instituto de Ciencia de Materiales de Madrid (CSIC). This work was supported in part by grants BIO2010-16351, BQU2009-08536, MAT2008-03232, from the Ministerio de Ciencia e Innovación (to J.F.D., J.J.B., and A.N., respectively) and National Natural Science Foundation of China (NSFC) grant 30930108 to W.S.F. The ESRF and the Netherlands Organization for Scientific Research (NWO) are gratefully acknowledged for beamtime on beamline BM26B (38) and the beamline staff is thanked for their support.

REFERENCES

1. Chrétien, D., F. Metoz, …, R. H. Wade. 1992. Lattice defects in microtubules: protofilament numbers vary within individual microtubules. *J. Cell Biol.* 117:1031–1040.
2. Montero, A., F. Fossella, …, V. Valero. 2005. Docetaxel for treatment of solid tumours: a systematic review of clinical data. *Lancet Oncol.* 6:229–239.
3. Buey, R. M., I. Barasoain, …, J. F. Díaz. 2005. Microtubule interactions with chemically diverse stabilizing agents: thermodynamics of binding to the paclitaxel site predicts cytotoxicity. *Chem. Biol.* 12:1269–1279.
4. Schiff, P. B., and S. B. Horwitz. 1981. Taxol assembles tubulin in the absence of exogenous guanosine 5′-triphosphate or microtubule-associated proteins. *Biochemistry* 20:3247–3252.
5. Díaz, J. F., and J. M. Andreu. 1993. Assembly of purified GDP-tubulin into microtubules induced by taxol and taxotere: reversibility, ligand stoichiometry, and competition. *Biochemistry* 32:2747–2755.
6. Wu, Z., H.-W. Wang, …, J. Xing. 2009. Simulations of tubulin sheet polymers as possible structural intermediates in microtubule assembly. *PLoS ONE* 4:e7291.
7. VanBuren, V., L. Cassimeris, and D. J. Odde. 2005. Mechanochemical model of microtubule structure and self-assembly kinetics. *Biophys. J.* 89:2911–2926.
8. Díaz, J. F., J. M. Andreu, …, J. Bordas. 1996. Structural intermediates in the assembly of taxoid-induced microtubules and GDP-tubulin double rings: time-resolved X-ray scattering. *Biophys. J.* 70:2408–2420.
9. Erickson, H. P. 1974. Microtubule surface lattice and subunit structure and observations on reassembly. *J. Cell Biol.* 60:153–167.
10. Chrétien, D., S. D. Fuller, and E. Karsenti. 1995. Structure of growing microtubule ends: two-dimensional sheets close into tubes at variable rates. *J. Cell Biol.* 129:1311–1328.
11. Vitre, B., F. M. Coquelle, …, I. Arnal. 2008. EB1 regulates microtubule dynamics and tubulin sheet closure in vitro. *Nat. Cell Biol.* 10:415–421.
12. Höög, J. L., S. M. Huisman, …, D. Brunner. 2011. Electron tomography reveals a flared morphology on growing microtubule ends. *J. Cell Sci.* 124:693–698.
13. Andreu, J. M., J. Bordas, …, E. Towns-Andrews. 1992. Low resolution structure of microtubules in solution. Synchrotron X-ray scattering and electron microscopy of taxol-induced microtubules assembled from purified tubulin in comparison with glycerol and MAP-induced microtubules. *J. Mol. Biol.* 226:169–184.
14. Andreu, J. M., J. F. Díaz, …, J. Bordas. 1994. Solution structure of Taxotere-induced microtubules to 3-nm resolution. The change in protofilament number is linked to the binding of the taxol side chain. *J. Biol. Chem.* 269:31785–31792.
15. Díaz, J. F., J. M. Valpuesta, …, J. M. Andreu. 1998. Changes in microtubule protofilament number induced by Taxol binding to an easily accessible site. Internal microtubule dynamics. *J. Biol. Chem.* 273:33803–33810.
16. Díaz, J. F., R. Strobe, …, J. M. Andreu. 2000. Molecular recognition of taxol by microtubules. Kinetics and thermodynamics of binding of fluorescent taxol derivatives to an exposed site. *J. Biol. Chem.* 275:26265–26276.
17. Nogales, E., M. Whittaker, …, K. H. Downing. 1999. High-resolution model of the microtubule. *Cell* 96:79–88.
18. Díaz, J. F., I. Barasoain, …, J. M. Andreu. 2005. Macromolecular accessibility of fluorescent taxoids bound at a paclitaxel binding site in the microtubule surface. *J. Biol. Chem.* 280:3928–3937.
19. Buey, R. M., E. Calvo, …, J. F. Díaz. 2007. Cyclostreptin binds covalently to microtubule pores and lumenal taxoid binding sites. *Nat. Chem. Biol.* 3:117–125.
20. Barasoain, I., A. M. García-Carril, …, J. F. Díaz. 2010. Probing the pore drug binding site of microtubules with fluorescent taxanes: evidence of two binding poses. *Chem. Biol.* 17:243–253.
21. Canales, A., J. Rodríguez-Salarichs, …, J. F. Díaz. 2011. Insights into the interaction of discodermolide and docetaxel with tubulin. Mapping the binding sites of microtubule-stabilizing agents by using an integrated NMR and computational approach. *ACS Chem. Biol.* 6:789–799.
22. Amos, L. A., and J. Löwe. 1999. How Taxol stabilises microtubule structure. *Chem. Biol.* 6:R65–R69.
23. Matesanz, R., I. Barasoain, …, J. F. Díaz. 2008. Optimization of taxane binding to microtubules: binding affinity dissection and incremental construction of a high-affinity analog of paclitaxel. *Chem. Biol.* 15:573–585.

24. Souto, A. A., A. U. Acuña, …, F. Amat-Guerri. 1995. New fluorescent water-soluble taxol derivatives. *Angew. Chem. Int. Ed. Engl.* 34:2710–2712.

25. Andreu, J. M., M. J. Gorbunoff, …, S. N. Timasheff. 1984. Interaction of tubulin with bifunctional colchicine analogues: an equilibrium study. *Biochemistry* 23:1742–1752.

26. Abramowitz, M., and I. A. Stegun. 1965. Handbook of Mathematical Functions. Dover Publications, New York.

27. Case, D. A., T. E. Cheatham, 3rd, …, R. J. Woods. 2005. The Amber biomolecular simulation programs. *J. Comput. Chem.* 26:1668–1688.

28. Sanner, M. F., A. J. Olson, and J. C. Spehner. 1996. Reduced surface: an efficient way to compute molecular surfaces. *Biopolymers* 38:305–320.

29. Pettersen, E. F., T. D. Goddard, …, T. E. Ferrin. 2004. UCSF Chimera—a visualization system for exploratory research and analysis. *J. Comput. Chem.* 25:1605–1612.

30. Jayalakshmi, V., and N. R. Krishna. 2002. Complete relaxation and conformational exchange matrix (CORCEMA) analysis of intermolecular saturation transfer effects in reversibly forming ligand-receptor complexes. *J. Magn. Reson.* 155:106–118.

31. Snyder, J. P., J. H. Nettles, …, E. Nogales. 2001. The binding conformation of Taxol in β-tubulin: a model based on electron crystallographic density. *Proc. Natl. Acad. Sci. USA* 98:5312–5316.

32. Magnani, M., G. Maccari, …, M. Botta. 2009. Possible binding site for paclitaxel at microtubule pores. *FEBS J.* 276:2701–2712.

33. Freedman, H., J. T. Huzil, …, J. A. Tuszynski. 2009. Identification and characterization of an intermediate taxol binding site within microtubule nanopores and a mechanism for tubulin isotype binding selectivity. *J. Chem. Inf. Model.* 49:424–436.

34. Canales, A., R. Matesanz, …, J. Jiménez-Barbero. 2008. The bound conformation of microtubule-stabilizing agents: NMR insights into the bioactive 3D structure of discodermolide and dictyostatin. *Chemistry* 14:7557–7569.

35. Díaz, J. F., I. Barasoain, and J. M. Andreu. 2003. Fast kinetics of Taxol binding to microtubules. Effects of solution variables and microtubule-associated proteins. *J. Biol. Chem.* 278:8407–8419.

36. Mitra, A., and D. Sept. 2008. Taxol allosterically alters the dynamics of the tubulin dimer and increases the flexibility of microtubules. *Biophys. J.* 95:3252–3258.

37. Alcaraz, A. A., A. K. Mehta, …, J. P. Snyder. 2006. The T-Taxol conformation. *J. Med. Chem.* 49:2478–2488.

38. Bras, W., I. P. Dolbnya, …, E. Heeley. 2003. Recent experiments on a combined small-angle/wide-angle X-ray scattering beam line at the ESRF. *J. App. Cryst.* 36:791–794.